Title: **Vertical 2D/3D Semiconductor Heterostructures Based on Epitaxial Molybdenum Disulfide and Gallium Nitride**

Authors: Dmitry Ruzmetov[1,3], Kehao Zhang[2], Gheorghe Stan[3], Berc Kalanyan[3], Ganesh R. Bhimanapati[2], Sarah M. Eichfeld[2], Robert A. Burke[1], Pankaj B. Shah[1], Terrance P. O'Regan[1], Frank J. Crowne[1], A. Glen Birdwell[1], Joshua A. Robinson[2], Albert V. Davydov[3], Tony G. Ivanov[1]

Affiliations:

1. Sensors and Electron Devices Directorate, US Army Research Laboratory, Adelphi, MD 20783, USA.

2. Department of Materials Science and Engineering & Center for Two-Dimensional and Layered Materials, The Pennsylvania State University, University Park, PA 16802, USA.

3. Material Measurement Laboratory, National Institute of Standards and Technology, Gaithersburg, MD 20899, USA.

Date: Wednesday, February 10, 2016

Supporting Information.

1. MoS_2 growth and substrate quality

The MoS_2 was grown on GaN substrate *via* powder vaporization technique. 2 mg MoO_3 (99.8%, Sigma Aldrich) is placed in the center of a single zone furnace, and 200mg sulfur powder (99.995%, Alfa Aesar) is located ~12 inch upstream of the MoO_3 crucible. Before starting growth a 10 minute vacuum (0.018 Torr) anneal at 300˚C was used to eliminate water and organic residuals in the furnace. Sulfur was heated at 130˚C immediately after the annealing. The growth temperature was then set at 800˚C and 710 Torr for 15 minutes with 100sccm ultra-pure argon flow. The schematic of the full temperature ramp profile of the furnace during the growth is shown in Figure S1.

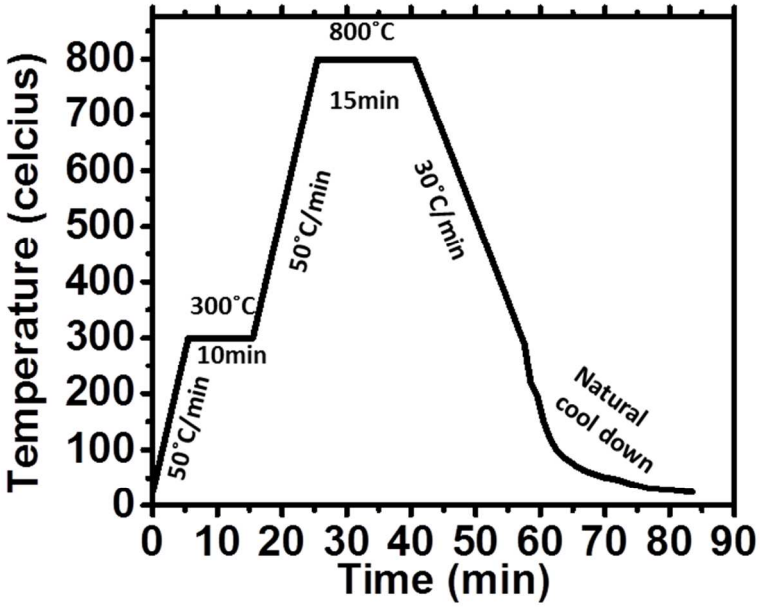

Figure S1. The temperature ramp profile of the CVD furnace during the growth of MoS_2 on GaN. The growth occurs at 800°C.

The roughness of GaN substrate has significant impact on the MoS_2 film quality. As an example, two types of GaN substrates were tested for the MoS_2 growth: a) Sapphire(c-plane)//GaN(HVPE, 5.5µm thick, free hole density p=1.2e18cm^{-3}, Mg-doped) and b) Sapphire(c-plane)//GaN(MOCVD, 700nm thick, epitaxial, free electron density n=1e19cm^{-3}, Si-doped)/GaN(MOCVD, 300nm thick, epitaxial, n=1e16cm^{-3}, Si-doped). The HVPE substrate was grown by hydride vapour phase epitaxy and the MOCVD substrate was grown by metalorganic chemical vapour deposition. The quality of the GaN substrates before the MoS_2 growth was analyzed by atomic force microscopy (AFM), see Figure S2a,b. The p-GaN substrate was measured to be significantly more rough (arithmetic average of absolute values surface roughness Ra=0.70nm) and has particles on the surface as compared to the n-GaN substrate (Ra=0.21nm). The CVD growth of MoS_2 was performed on both types of substrates using procedures similar to what we described above. The scanning electron microscopy (SEM, Figure S2c) and AFM (Figure S2e) analysis of the MoS_2 growth on the p-GaN substrate shows mostly the absence of the oriented 2D growth with characteristic thicknesses of MoS_2 structures of 5nm. At the same time, the MoS_2 grown on smooth n-GaN substrates shows epitaxial alignment and monolayer thicknesses.

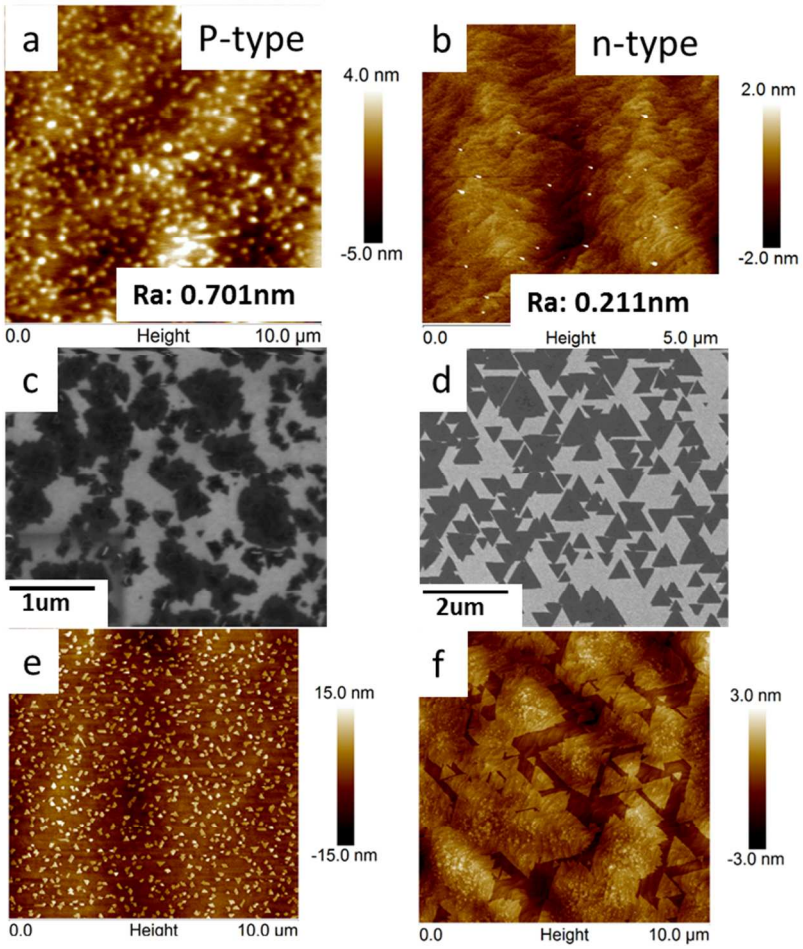

Figure S2. Comparison of the MoS_2 growth on the GaN substrates of different roughness. AFM maps of bare GaN substrates grown by (a) HVPE, p-GaN, and (b) MOCVD, n-GaN. SEM images of the resulting MoS_2 structures on (c) p-GaN and (d) n-GaN. AFM maps of MoS_2 on (e) p-GaN and (f) n-GaN.

2. Raman and Photoluminescence

Raman and photoluminescence (PL) spectroscopy has been utilized extensively to investigate MoS_2 from a few molecular layers (MLs) down to a single-molecular layer (SML)[1,2]. Here, we provide a very brief review detailing some of the information made available by these techniques.

The Raman spectra are dominated by two characteristic Raman-active modes, noted as the in-plane E^1_{2g} and the out-of-plane A_{1g} modes in few layer systems. Since there is no center of inversion for a SML of MoS_2, E' and A'_1 are used instead of the common E^1_{2g} and A_{1g} notations when reference is made to the SML in this work. One of the most distinctive properties of confining the system to fewer layers is the redshift of the A_{1g} mode and blueshift of the E^1_{2g} phonon mode with decreasing number of layers. The blueshift of the E^1_{2g} peak was shown to be due to dielectric screening of the long-range Coulomb interaction,[3] while the redshift of the A_{1g} mode is in line with the classical picture of a harmonic potential.[4] As such, the frequency difference between E^1_{2g} and A_{1g} is often used to identify the number of MoS_2 layers. These two characteristic Raman modes have phonon frequency in the SML limit of ~385 cm^{-1} and ~405 cm^{-1}, respectively.

Other perturbations can also affect the peak positions of these characteristic phonon modes, e.g., strain and doping.[5,6] Work concerning the effect of strain shows that the in-plane E^1_{2g} mode is sensitive to strain, while the out-of-plane A_{1g} mode shows a weak strain dependence.[5] These two modes show distinct doping dependence; with the A_{1g} mode decreasing in frequency with increased electron concentration, and the E^1_{2g} mode showing an overall weak dependence on electron concentration.[6] This difference is attributed to the stronger coupling to electrons of the A_{1g} mode compared with the E^1_{2g} mode. As a final point, recent work by Zhou and coworkers demonstrate that a blueshift of the A_{1g} mode is indicative of the strength of the van der Waals contact with the adjacent substrate.[7]

The conversion of an indirect gap material to one with a direct gap when the layer count is reduced to a single-molecular layer (SML) is one of the most astonishing features of many layered van der Waals materials such as MoS_2.[8,9] Reduction to a SML of MoS_2 results in considerable light emission due to direct exciton recombination at a photon energy of ~1.8-1.9 eV. This photon energy is significantly lower than the first direct gap due to the existence of a very strong binding energy of the 2D excitons as recently demonstrated by several research groups.[10–12] Two distinct peaks in the PL spectra may be observed near this energy range and are due to spin-orbit-induced splitting of the valence band. The most intense and lowest energy feature is known as the "A" exciton peak, whereas the much lower intensity and higher energy peak is the "B" exciton. The A-exciton peak is the PL feature of interest in this study. It should be noted that the intensity of A-exciton peak can be highly variable and is dependent upon the host substrate.[13] Furthermore, a considerable PL enhancement can result from physisorption of certain molecules that act as p-type dopants.[14] The energy position and width (FWHM) of this PL peak provides useful information related to the layer count, strain-state, and structural quality of the 2D layer.

Figure S3(a,b,c) displays optical, Raman, and PL images taken at a region where small triangles have merged into continuous SMLs or layer stacks of 2 or more MLs. This region is chosen to demonstrate the high selectivity of Raman and PL dependence on the layer count. Features in the Raman image (Figure S3b) are indicative of increased layer thickness with the greatest intensity originating from regions with the largest number of layers. Features in the PL image (Figure S3c) corroborate those observed with Raman with regions of no-growth (black regions), SML growth (bright regions), and 2 or more MLs (grey

regions) easily identifiable. The colored circles with white outline note points where single spectra were taken and were shown in the main text in Figure 2e,f.

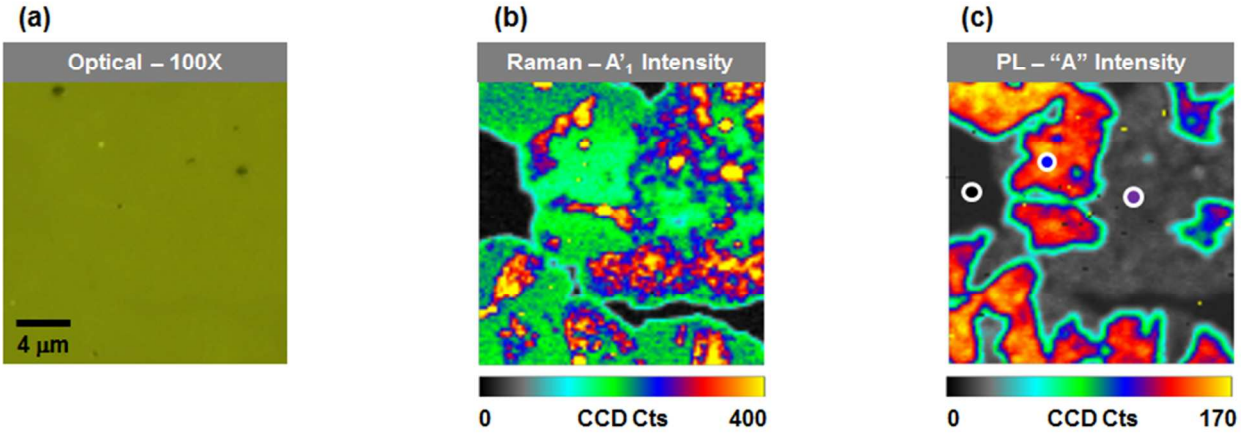

Figure S3. (a) Optical micrograph, (b) Raman image of the A'_1 mode intensity, and (c) PL image of the intensity of "A" exciton peak taken at a region where small triangles have merged into continuous SMLs or layer stacks of 2 or more MLs.

Table S1. Raman spectral parameters corresponding to spectra shown in Figure 2e in the main text.

	E' or E^1_{2g} Mode (cm^{-1})		**A'_1 or A_{1g} Mode (cm^{-1})**	
Structure	**Peak Position**	**FWHM**	**Peak Position**	**FWHM**
ME MoS_2/SiO_2	386.5	5.5	405.4	6.4
MoS_2/GaN – Large Triangle	386.5	6.6	406.3	6.5
MoS_2/GaN – Continuous SML	385.7	6.6	406.2	6.8
MoS_2/GaN – 2-Molecular Layers	384.5	7.5	407.1	7.1

Table S2. Photoluminescence spectral parameters corresponding to spectra shown in Figure 2f in the main text. The ratio of the PL intensity (I_{lum}) and Raman intensity (I_{Raman}) is used as a measure of the intrinsic luminescence quantum efficiency as describe by Splendiani and coworkers.[8]

	"A" Exciton		
Structure	**Peak Position (eV)**	**FWHM (meV)**	**I_{Lum}/I_{Raman}**
ME MoS_2/SiO_2	1.875	91	16
MoS_2/GaN – Large Triangle	1.883	63	400
MoS_2/GaN – Continuous SML	1.868	82	17
MoS_2/GaN – 2-Molecular Layers	1.845	116	3

3. Conductive atomic force microscopy study

Conductive atomic force microscopy (CAFM) as well as other types of atomic force microscopy (AFM) were used to characterize the MoS_2 structures on GaN. The details on the CAFM and AFM techniques and nano-probes (tips) used are given in the Methods section of the main text. During a CAFM measurement a CAFM tip was grounded and served as the top nano-electrode while the degenerately n-doped GaN layer on the substrate was biased and served as the bottom contact to the MoS_2/GaN stacks, as depicted in the measurement diagram in Figure 4a. Large area (A_{back}) Ti(bottom)/Au pads near the edges of the sample were evaporated on the top of the GaN wafer and served as the contacts to the bottom electrode, n^+GaN. Evaporation of the contacts with shadow masks allowed to avoid the contact of the samples with microfabrication chemicals. The Ti/Au contacts were non-ohmic but introduced only insignificant (due to large $A_{back} \gg A_c$) contact resistance ($R_{back} \propto A_{back}^{-1}$) below 1 kΩ thus contributing negligible uncertainty (< 6 μV) to the tip-to-n^+GaN bias at the currents measured.

In CAFM areal imaging, the substrate was biased at a constant voltage and the measured current was mapped. Topographical AFM imaging that included phase contrast imaging was usually performed over the area selected for the CAFM current mapping. A topographic map and corresponding current map of the MoS_2 structures on GaN substrate are displayed in Figure S4. The amplitude modulation AFM maps of the topography and phase contrast are displayed in Figure S5. Phase contrast images readily distinguish MoS_2-covered areas from GaN surface. The topographic images display a terrace-like structure of the GaN substrate with ultra-thin triangles and blankets of MoS_2 scattered on the surface. A topographic line scan across a MoS_2 triangle is shown in Figure S4 with a vertical step in the place of the triangle just standing out from the background noise and consistent with 0.7 ± 0.5 nm height. Second layer triangles and higher order growth can be readily seen in topographic AFM images (Figure S5) due to lower noise level on the MoS_2 structures and measure approximately 0.7 nm per monolayer. Areal and line CAFM scans at -7V substrate bias shown in Figure S4b display the increase of conductivity on the MoS_2 triangles and the uniform current level throughout the triangles likely due to the current spreading in the MoS_2 layer. There are obvious fluctuations in the current level outside the triangles and on the GaN substrate (Figure S4b). Secondary electron microscopy (SEM) analysis of the GaN substrate areas in between the MoS_2 triangles reveals some disordered, nanoscale growth structures in the form of clusters of nano-particles visible only at high magnification. The topographic AFM analysis shows that those nascent, disordered growth structures, if present, must be generally no more than a MoS_2 monolayer in height. The nature of the observed nanoscale growth on GaN is unclear and it may be either a sub-monolayer of MoS_2 that later develops into ML MoS_2 or another material such as MoO_x. We speculate that those current fluctuations in the CAFM areal image (Figure S4b) come from the enhancement of the conduction on nanoscale growth structures on the GaN substrate.

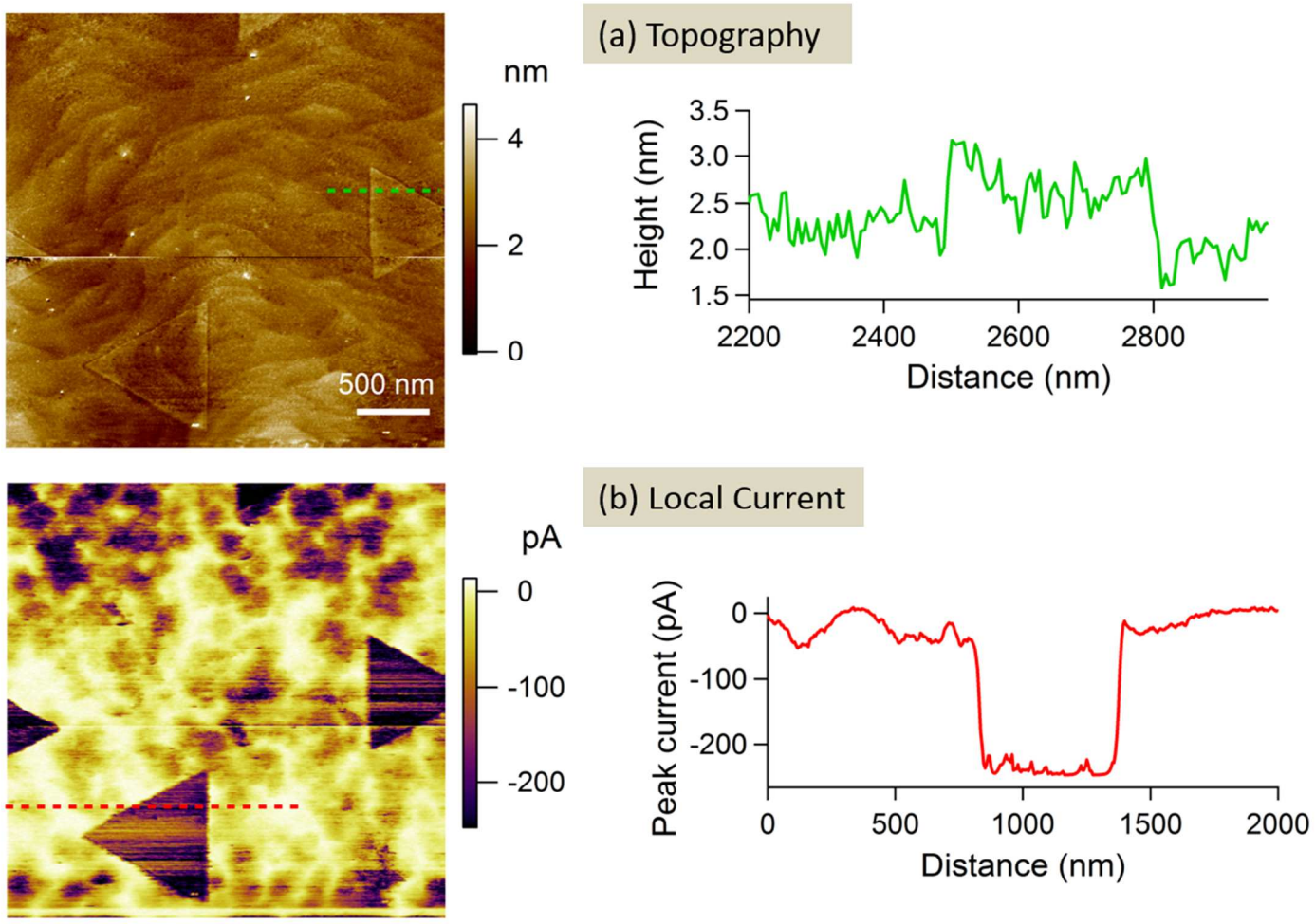

Figure S4. Conductive AFM measurements on MoS_2. (a) Topography map and a line scan (b) Local current map and a line scan across a MoS_2 triangle. The current and conductivity are enhanced on the MoS_2 monolayer triangles.

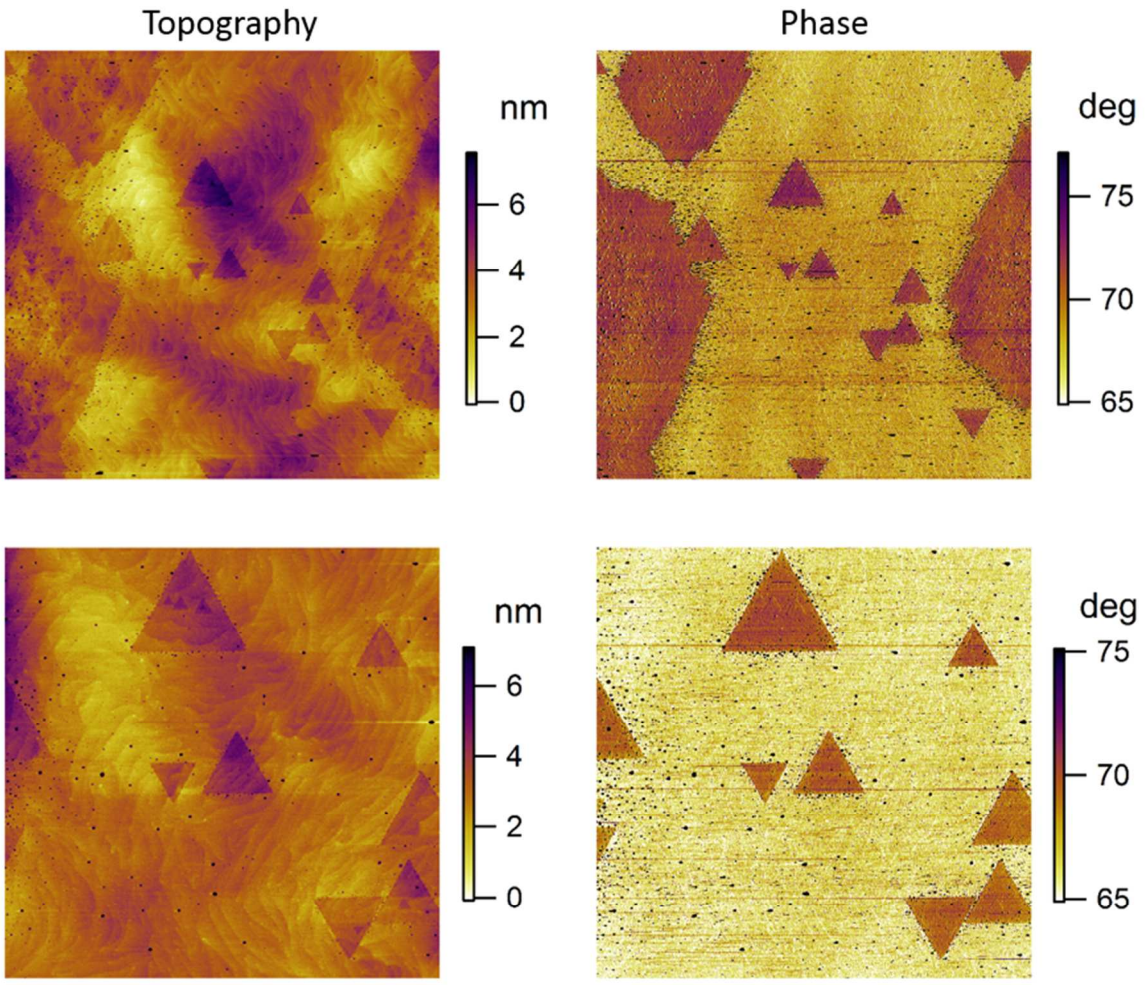

Figure S5. AFM characterization of the MoS_2 on GaN terraced surface. (Left) Topography maps point out the higher order layer count. (Right) The phase maps distinguish between MoS_2 and GaN. (Top) Map size 10um x 10um. (Bottom) 5um x 5um.

I-V spectroscopy at selected points on the sample surface was performed with the CAFM tip. Typical measured current-voltage curves for the MoS_2 monolayer and GaN substrate are displayed in Figure S6a. The voltage polarity on the graphs in Figure S6 is chosen so that the positive voltage corresponds to the forward Schottky bias, i.e. electrons are injected from the semiconductor sample to the conductive tip.

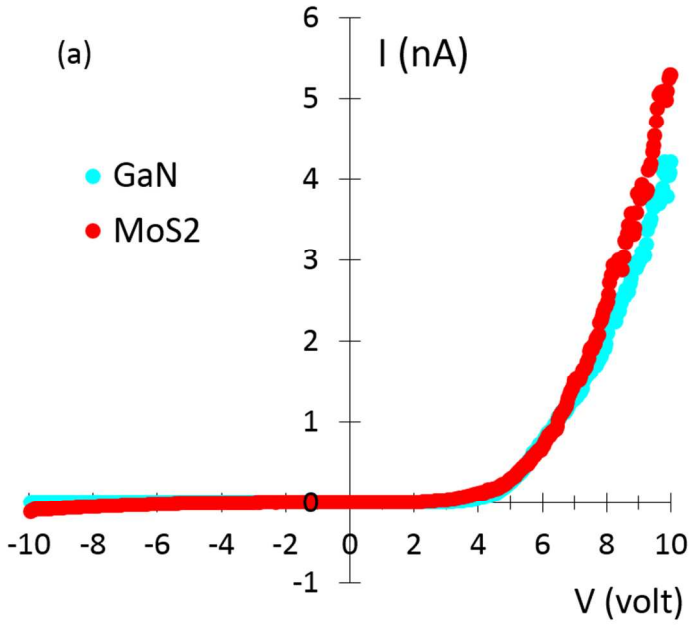

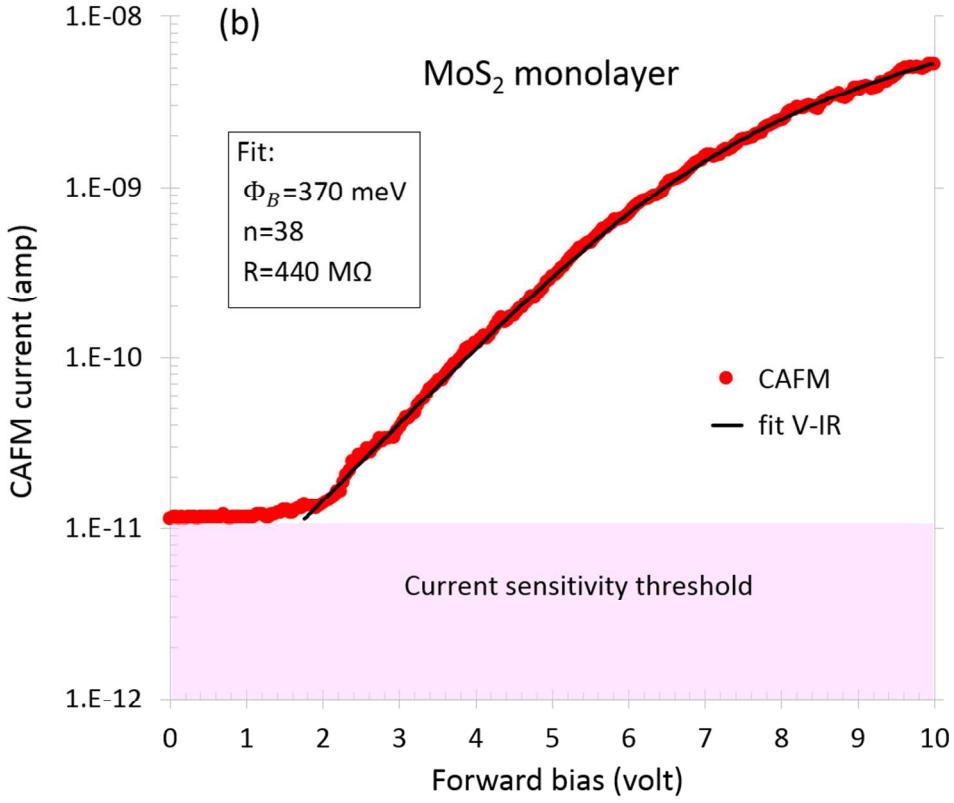

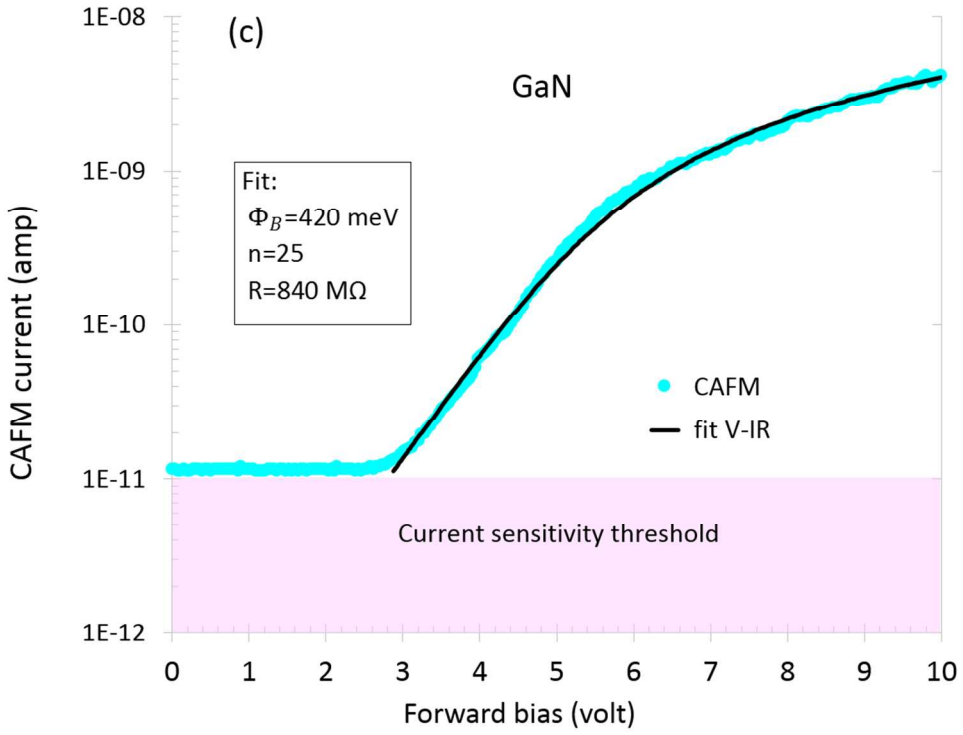

Figure S6. Current spectroscopy of the tip/MoS_2/GaN and tip/GaN structures with fitting using the equation (1).

The current-voltage curves for the point CAFM measurements on both MoS_2 and bare GaN substrate display rectifying behavior (Figure S6a) suggesting that interfaces, not the bulk, are dominant contributors to the resistance. The similar current range and the shape of the MoS_2 and GaN curves and the expectation of the nGaN/n^+GaN contact to be close to ohmic suggest that the I-V behavior is mostly set by the non-ohmic contact between the CAFM tip and the sample. The I-V curves on MoS_2 locations display higher currents and narrower location-to-location variation than the I-V curves at the GaN locations. Since the I-V measurements on GaN might be affected by the nanoscale growth structures described earlier in this section and that are unresolved in the AFM images, we focus our analysis of the I-V spectroscopy on the data from MoS_2 monolayers and show the data from the bare GaN locations only for comparison.

In order to de-convolute the embedded information on the MoS_2/GaN interface we analyzed the I-V curves at forward bias as shown in Figure S6b,c. At low bias voltages the current stays at the instrumental threshold level (approximately 10pA). From the threshold to 0.5 nA the I-V follows the exponential rise that starts saturating above 1nA. The same trend is true for the I-V curves of GaN. The current injection from a CAFM tip to a MoS_2 multilayer has been successfully described by Giannazzo *et al.* with the model of thermionic emission over the Schottky barrier[15]:

$$I = A_{tip} A^* T^2 e^{-\frac{q\Phi_B}{kT}} e^{\frac{q(V-IR)}{nkT}}, \qquad (1)$$

where *V* is the applied bias between the tip and the sample, *R* is the resistance contributing to the voltage drop between the back contact to the sample and the tip-semiconductor interface, A_{tip} is the tip-sample contact area, $A^* = 4\pi q k^2 m_{eff}/h^3$ is the Richardson constant with m_{eff} - effective mass

for electrons, h - Planck constant, T=293 K - the ambient temperature, q - elementary charge, Φ_B - height of the Schottky barrier at the tip-semiconductor interface measured from the Fermi level in the tip, k - Boltzmann constant, n - the ideality factor. We employed the formula (1) to fit all the I-V curves for MoS_2 and GaN with $A_{tip} \approx 100\ nm^2$[16] and the effective masses m_{eff} of $0.47\ m_e$ for monolayer MoS_2[17] and $0.20\ m_e$ for wurtzite GaN. Typical fitting results are displayed in Figure S6b,c. For the low currents (below 0.6 nA) the curves could be fit with a simple exponent described with two fitting parameters (Φ_B, n, R=0). At larger currents the I·R correction needed to be added to account for the discrepancy between the applied voltage and the voltage across the tip-semiconductor Schottky barrier. The extracted fitting parameters are Φ_B=370 meV, n=38, R=440 MΩ for MoS_2 and Φ_B=420 meV, n=25, R=840 MΩ for GaN. Large ideality factors raise a question on the applicability of the thermionic emission model for the tip-semiconductor contacts, suggesting that the extracted Schottky barrier heights need to be considered with caution. Nevertheless our value of Φ_B=370 meV for the barrier between monolayer MoS_2 and a doped diamond tip is not far from the reported Φ_B=307 meV for the multilayer MoS_2 and Pt-coated AFM tip[15]. The larger resistance R=840 MΩ for the GaN substrate is likely due to the smaller injection area in the top GaN and GaN/n^+GaN interface. The value of R=440 MΩ for MoS_2 includes the contact resistance of the MoS_2/GaN interface and is used in the main text to estimate the upper bound of the interface's contact resistivity.

Different types of AFM characterizations (topography, adhesion, and electrical surface potential) of the same MoS_2 triangle are displayed in Figure S7. The MoS_2 triangle exhibits higher adhesion to the CAFM tip than GaN. The presence of nano-dots (discussed in the main text as topographic spikes) is clearly visible in the topography and adhesion images at the perimeter of the triangle. The nano-dots are isolated and 3 to 5 nm in height and not to be confused with the sub-monolayer nanoscale growth contributing to the enhanced conductivity of the tip on GaN that is mentioned earlier in this section. The nano-dots are scattered over the GaN surface and have high density at the edges of the triangle. It is likely that the nano-dots are the re-deposition of MoO_x. The accumulation of the nano-dots near the edges might be due to the higher density of defect-related nucleation centers there.

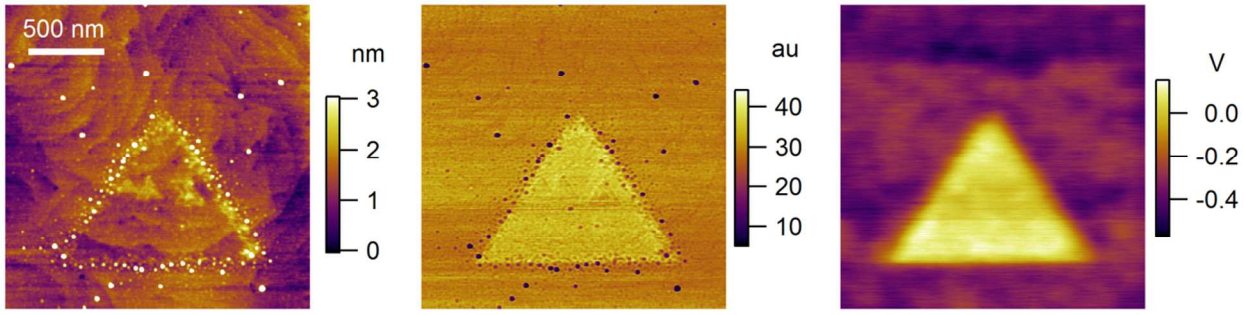

Figure S7. Topography, adhesion, and surface potential map of a MoS_2 triangle with some bilayer and trilayer growth.

4. X-ray photoelectron spectroscopy analysis

We measured three unique spots on MoS_2 /GaN in order to investigate how the material composition changes with the density of the MoS_2 structures (Figure S8). Concentration of Mo and S atoms (from Mo 3d and S 2s) increase in unison as measured from the downstream end of the wafer toward the upstream region (with respect to gas flow in the CVD furnace). This indicates that the MoS_2 concentration is higher for regions of the wafer closer to the precursor source. We observed the same trend with SEM measurements, where regions of the wafer close to the CVD source crucible show higher MoS_2 coverage. The ratio of MoO_x to MoS_2 decreases toward the upstream end of the wafer, as shown in Figure S8a. As the MoS_2 domains grow larger, the contribution of the MoO_x to the total Mo 3d signal diminishes. This is in accord with the picture where MoO_x redeposition is happening mostly on the bare GaN substrate. Also, this agrees with MoO_x nature of the nano-dots shown in Figure S7 since the density of the nano-dots is lower inside the MoS_2 structures. The deconvoluted O 1s spectra are shown in Figure S8e. We ascribe the low binding energy O 1s component (530.8 eV) to MoO_x, similar to previous measurements of Mo oxides[18]. The higher binding energy peak (532 eV) is related to oxidized surface carbon, since this peak tracks in intensity with the C 1s peak at 285.2 eV in Figure S8d.

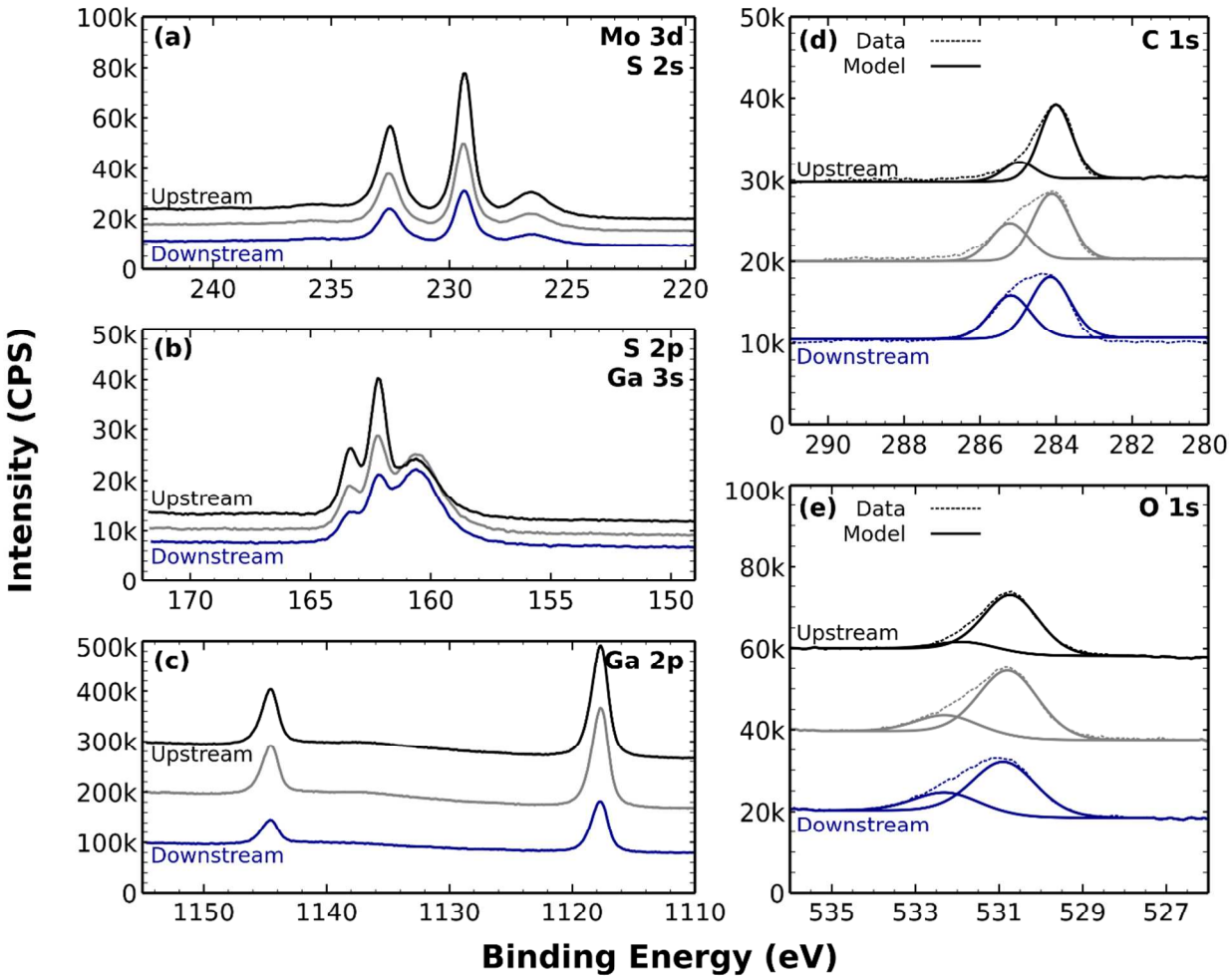

Figure S8. Comparison of Mo 3d, S 2s, S 2p, Ga 3s, Ga 2p, C 1s, and O 1s regions for upstream and downstream spots on the MoS_2/GaN/n-GaN/Sapphire stack.

As discussed in the main text, we evaluated the stability of GaN during CVD processing using a special CVD run. We ran a GaN/GaN/Sapphire wafer through the CVD process without loading the MoO_3 precursor. We compared this wafer to unprocessed GaN and to MoS_2/GaN. We first calculated the modified Auger parameters (α') for O 1s,KLL and Ga 3d,$L_3M_{45}M_{45}$ for each condition (Table S3), where the parameter is defined as the sum of the Auger transition kinetic energy and the core level peak binding energy. The parameter is a means of comparing the chemical state of a specific component, independent of differential charging effects.

Table S3. Auger parameter (A.P.) for oxygen and gallium from GaN, GaN+S, and GaN+MoS_2 surfaces.

Surface	O A.P.-1s,KLL (eV)	Ga A.P.-3d,$L_3M_{45}M_{45}$ (eV)
GaN	1042.5±0.2	1084±0.01
GaN + S	1042.8±0.2	1084.1±0
GaN + MoS_2	1042.3±0.2	1084.1±0.01

For oxygen, α' varies from 1042.3 to 1042.8 eV, which suggest that oxygen is primarily found in hydrocarbon form. Evidence for oxidized gallium is notably absent both in terms of Auger parameter values (α' for O 1s of Ga_2O_3 is expected to be 1041.4 eV[19]) and in the Ga core levels. Likewise, Ga α' values are consistent with GaN[19,20]. Since the MoS_2 overlayer is thin enough to be transparent to Ga photoelectrons, the lack of evidence for Ga_2O_3 indicates that the MoS_2/GaN interface is not oxidized during CVD. It is possible that the oxygen from the MoO_3 precursor is converted entirely into volatile SO_2 as a by-product of the MoS_2 growth[21]. On the other hand, the GaN surface subjected to a sulfur atmosphere at 800°C shows a small degree of sulfurization (1.3±0.1 atomic%, Table S4). A weak S 2s peak is detectable at 226.4 eV. Since the Auger parameters for GaN and gallium chalcogenides are very close, the exact assignment of this sulfur peak is difficult. Furthermore, the Ga 3s peak (Figure S9) completely obscures small S 2p doublets that may be expected in this region. Therefore, we cannot readily determine the identity of the S species on the surface.

Table S4. Atomic compositions measured by XPS for unprocessed (GaN), sulfur-exposed (GaN + S), and MoS_2-coated (GaN + MoS_2) GaN/GaN/Sapphire surfaces. Percentages are calculated using C 1s, Ga 3p, N 1s, O 1s, Mo 3d, and S 2s peaks. Each percentage is an average of three measurements.

	%C	%Ga	%N	%O	%Mo	%S
GaN	9.2 ± 0.6	44.8 ± 0.7	39.2 ± 0.4	6.8 ± 0.5	0 ± 0	0 ± 0
GaN + S	13.3 ± 0.6	41.9 ± 0.2	34.2 ± 0.4	9.2 ± 0.2	0 ± 0	1.3 ± 0.1
GaN + MoS_2	12.6 ± 1.5	34.1 ± 2.4	29.1 ± 2.8	8.8 ± 0.6	5.1 ± 2.5	10.3 ± 4.6

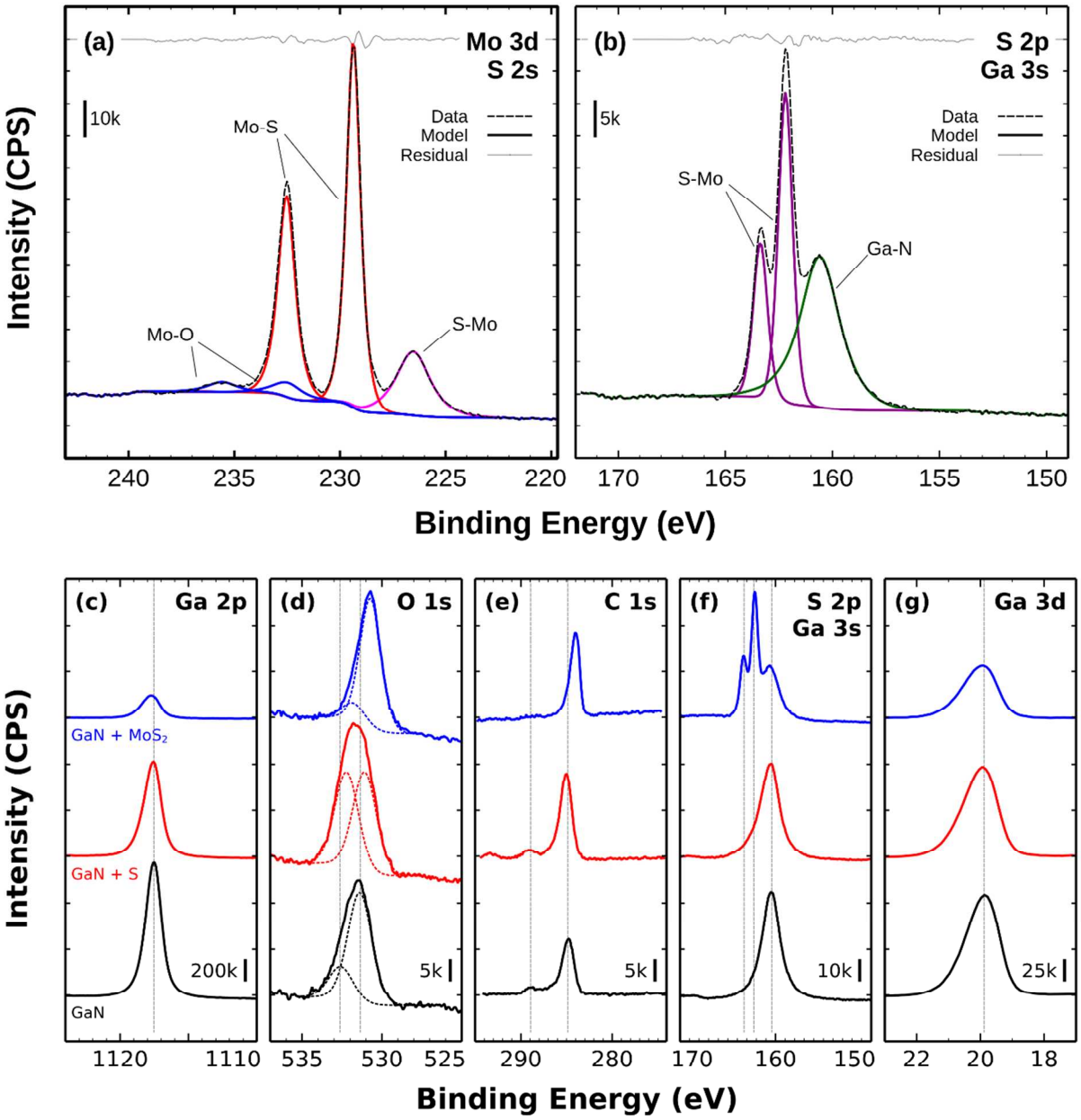

Figure S9. Core level spectra from (a) Mo 3d and (b) S 2p regions of MoS_2 on GaN. Panel (a) shows components from S 2s (MoS_2), Mo $3d_{5/2}$ and $3d_{3/2}$ doublets (MoS_2 and MoO_x). In (b), the S 2p doublet (MoS_2) and Ga 3s (GaN) are shown. Panels (c), (d), (e), (f), and (g) show a comparison of Ga 2p, O 1s, C 1s, S 2p, Ga 3s, and Ga 3d regions for the unprocessed GaN surface (bottom traces, black), GaN exposed to sulfur (middle traces, red), and GaN+MoS_2 (top traces, blue).

References

1. Lee, C.; Yan, H.; Brus, L. E.; Heinz, T. F.; Hone, J.; Ryu, S. Anomalous Lattice Vibrations of Single-and Few-Layer MoS2. *ACS Nano* **2010**, *4*, 2695–2700.
2. Li, H.; Zhang, Q.; Yap, C. C. R.; Tay, B. K.; Edwin, T. H. T.; Olivier, A.; Baillargeat, D. From Bulk to Monolayer MoS2: Evolution of Raman Scattering. *Adv. Funct. Mater.* **2012**, *22*, 1385–1390.

3. Molina-Sanchez, A.; Wirtz, L. Phonons in Single-Layer and Few-Layer MoS2 and WS2. *Phys. Rev. B* **2011**, *84*, 155413.
4. Lanzillo, N. A.; Birdwell, A. G.; Amani, M.; Crowne, F. J.; Shah, P. B.; Najmaei, S.; Liu, Z.; Ajayan, P. M.; Lou, J.; Dubey, M.; Nayak, Saroj K.; O'Regan, Terrance P. Temperature-Dependent Phonon Shifts in Monolayer MoS2. *Appl. Phys. Lett.* **2013**, *103*, 093102.
5. Rice, C.; Young, R. J.; Zan, R.; Bangert, U.; Wolverson, D.; Georgiou, T.; Jalil, R.; Novoselov, K. S. Raman-Scattering Measurements and First-Principles Calculations of Strain-Induced Phonon Shifts in Monolayer MoS2. *Phys. Rev. B* **2013**, *87*, 081307.
6. Chakraborty, B.; Bera, A.; Muthu, D. V. S.; Bhowmick, S.; Waghmare, U. V.; Sood, A. K. Symmetry-Dependent Phonon Renormalization in Monolayer MoS2 Transistor. *Phys. Rev. B* **2012**, *85*, 161403.
7. Zhou, K.-G.; Withers, F.; Cao, Y.; Hu, S.; Yu, G.; Casiraghi, C. Raman Modes of MoS2 Used as Fingerprint of van Der Waals Interactions in 2-D Crystal-Based Heterostructures. *ACS Nano* **2014**, *8*, 9914–9924.
8. Splendiani, A.; Sun, L.; Zhang, Y.; Li, T.; Kim, J.; Chim, C.-Y.; Galli, G.; Wang, F. Emerging Photoluminescence in Monolayer MoS2. *Nano Lett.* **2010**, *10*, 1271–1275.
9. Mak, K. F.; Lee, C.; Hone, J.; Shan, J.; Heinz, T. F. Atomically Thin MoS2: A New Direct-Gap Semiconductor. *Phys. Rev. Lett.* **2010**, *105*, 136805.
10. Chernikov, A.; Berkelbach, T. C.; Hill, H. M.; Rigosi, A.; Li, Y.; Aslan, O. B.; Reichman, D. R.; Hybertsen, M. S.; Heinz, T. F. Exciton Binding Energy and Nonhydrogenic Rydberg Series in Monolayer WS2. *Phys. Rev. Lett.* **2014**, *113*, 076802.
11. Ugeda, M. M.; Bradley, A. J.; Shi, S.-F.; Felipe, H.; Zhang, Y.; Qiu, D. Y.; Ruan, W.; Mo, S.-K.; Hussain, Z.; Shen, Z.-X.; Wang, Feng; Louie, Steven G.; Crommie, Michael F. Giant Bandgap Renormalization and Excitonic Effects in a Monolayer Transition Metal Dichalcogenide Semiconductor. *Nat. Mater.* **2014**.
12. Li, W.; Birdwell, A. G.; Amani, M.; Burke, R. A.; Ling, X.; Lee, Y.-H.; Liang, X.; Peng, L.; Richter, C. A.; Kong, J.; Gundlach, David J.; Nguyen, N. V. Broadband Optical Properties of Large-Area Monolayer CVD Molybdenum Disulfide. *Phys. Rev. B* **2014**, *90*, 195434.
13. Li, Y.; Qi, Z.; Liu, M.; Wang, Y.; Cheng, X.; Zhang, G.; Sheng, L. Photoluminescence of Monolayer MoS2 on LaAlO3 and SrTiO3 Substrates. *Nanoscale* **2014**, *6*, 15248–15254.
14. Su, W.; Dou, H.; Li, J.; Huo, D.; Dai, N.; Yang, L. Tuning Photoluminescence of Single-Layer MoS2 Using H2O2. *RSC Adv* **2015**, *5*, 82924–82929.
15. Giannazzo, F.; Fisichella, G.; Piazza, A.; Agnello, S.; Roccaforte, F. Nanoscale Inhomogeneity of the Schottky Barrier and Resistivity in MoS2 Multilayers. *Phys. Rev. B* **2015**, *92*, 081307.
16. Yao, N.; Wang, Z. L. *Handbook of Microscopy for Nanotechnology*; Springer, 2005.
17. Yu, S.; Xiong, H. D.; Eshun, K.; Yuan, H.; Li, Q. Phase Transition, Effective Mass and Carrier Mobility of MoS2 Monolayer under Tensile Strain. *Appl. Surf. Sci.* **2015**, *325*, 27–32.
18. Leung, Y. L.; Wong, P. C.; Zhou, M. Y.; Mitchell, K. A. R.; Smith, K. J. XPS Studies of the Nitridation of MoO3 Thin Films on Alumina and Silica Supports. *Appl. Surf. Sci.* **1998**, *136*, 178–188.
19. NIST X-Ray Photoelectron Spectroscopy Database, Version 4.1 (National Institute of Standards and Technology, Gaithersburg); Http://srdata.nist.gov/xps/, **2012**.
20. Perry, D. L. Application of Combined X-Ray Photoelectron/Auger Spectroscopy to Studies of Inorganic Materials. In *Applications of Analytical Techniques to the Characterization of Materials*; Perry, D. L., Ed.; Springer US, 1991; pp. 1–23.
21. Senthilkumar, V.; Tam, L. C.; Kim, Y. S.; Sim, Y.; Seong, M.-J.; Jang, J. I. Direct Vapor Phase Growth Process and Robust Photoluminescence Properties of Large Area MoS2 Layers. *Nano Res.* **2014**, *7*, 1759–1768.